Identification of strongly nonlinear structures by displacement measurement

Qinghua Liu[a], Zehao Hou[a], Ying Zhang[a], Xingjian Jing[b], Gaetan Kerschen[c], Junyi Cao[a*]

[a] Key Laboratory of Education Ministry for Modern Design and Rotor-Bearing System, Xi'an Jiaotong University, Xi'an, China

[b] Department of Mechanical Engineering, The Hong Kong Polytechnic University, Hong Kong, China

[c] Department of Aerospace and Mechanical Engineering, University of Liege, Belgium

Abstract

Strongly nonlinear structures have attracted a great deal of attention in the field of energy harvesting and vibration isolation recently. However, it is challenging to accurately characterize the nonlinear restoring force by analytical modeling or direct measurement in many realistic conditions due to the uncertainty of installation parameters or some constraints, including space size and dynamic disturbance. Therefore, the displacement-measurement restoring force surface identification approach is presented for describing the nonlinear restoring force. The widely known quasi-zero stiffness, bistable and tristable structures are designed in the cantilever beam system with rotatable magnets coupling to illustrate strongly nonlinear properties in the application of energy harvesting and vibration isolation. Based on the derived physical model of the designed strongly nonlinear structures, the displacement-measurement restoring force surface identification with least-squares parameter fitting is proposed to obtain the nonlinear parameters of the stiffness force and damping force. The comparison between acceleration integration and displacement differentiation method for describing the restoring force surface of strongly nonlinear structures is discussed. Besides, the influence of noise level on identification accuracy is investigated. In experimental conditions, quasi-zero stiffness, bistable and tristable nonlinear structures with various geometrical parameters are performed to comparatively analyze the identified nonlinear stiffness force curve and measured force-displacement trajectory. Experimental results verify the

[*]Author to whom correspondence should be addressed. Electronic mail: caojy@mail.xjtu.edu.cn

effectiveness of the displacement-measurement restoring force surface method for describing the nonlinear stiffness force.

Keywords: Strongly nonlinear structures; Displacement-measurement restoring force surface; Quasi-zero stiffness; Bistable structure; Tristable structure.

1. Introduction

In recent years, many strongly nonlinear structures have been widely used in passive vibration isolation and energy harvesting. The basic principle of these nonlinear structures is to form an ideal nonlinear restoring force by coupling negative stiffness forces based on linear structures, such as oblique spring/bar [1,2], X-shaped structures [3,4], cam-roller-spring mechanisms [5,6], buckled beam [7,8] and magnetic coupling structures [9,10], etc. These nonlinear elements change the system's dynamic response and make it useful in many engineering occasions but increase the complexity of nonlinear stiffness force calculation or identification.

In the last decade, the popular methods of describing nonlinear restoring force include analytical calculation and direct measurement using the instrument. Carrella et al. calculated the force-displacement function of oblique spring-type high-static-low-dynamic-stiffness (HSLDS) isolator and then simplified it with cubic polynomial function to make great convenience for the analytical solution of dynamic equation [1]. Thanh et al. precisely characterized the nonlinear stiffness force of the HSLDS vehicle seat, and then Lagrange's equation was adopted for derivation of dynamic equation [2]. In complex spatial geometric structures such as diamond, X-shaped, and bionic structures invented by Jing et al., two common ways are either the purely mathematical calculation of nonlinear restoring force or using Lagrange's equation for modeling [3,4,11]. Zhou et al. utilized the cam-roller-spring mechanisms to construct quasi-zero stiffness force and replace the exact expression of nonlinear stiffness force with an approximate piecewise form to obtain the analytical solution of the system [5]. The above-mentioned analytical methods for nonlinear stiffness force calculation in vibration isolation structures are always based on the physical model with the ideal assumptions and be mathematically complicated. For bistable or tristable structures with

magnetic force coupling in energy harvesting, the magnetic dipoles theory, equivalent magnetic current and magnetic charge method were always used for analytical calculation of magnetic force [12-14]. However, these analytical approaches suffer from the limitations of magnet's dimensions and magnet's intervals, accurate calculation of magnetic field distribution along conductors and complex computations. Moreover, Zhou et al. and Leadenham et al. measured the nonlinear stiffness force of the multi-stable beams and an M-shaped piezoelectric energy harvester, respectively, then fitted it with empirical polynomial function for dynamic analysis [9,10,15]. However, it will lead to a failure in another system once any parameter changes or force measuring instruments cannot be installed and arranged.

In addition to analytical calculation and direct measurement, the identification strategy of nonlinear stiffness force such as the nonlinear subspace method and restoring force surface method has also received considerable interest in the recent decade [16]. For the nonlinear subspace-based method, the nonlinear restoring force is applied to the underlying linear system as a feedback force and then identifies the coefficients by frequency response function. Marchesiello et al. numerically studied this method to identify cubic and clearance type nonlinearities [17]. Later, this method and its improved version of the nonlinear frequency domain subspace algorithm have been widely used in aerospace structures, such as impacts on the mechanical stops [18], bolted connected joints on wingtip [19] and solar array structures [20]. However, the expression of nonlinear feedback force requires a priori knowledge to ensure the accuracy of identification. The restoring force surface method, or called force-state mapping, initially proposed by Masri and Caughey [21,22], has also been widely used in nonlinear force identification. Al-Hadid and Wright used the acceleration-measurement force-state mapping method to identify the weakly nonlinear T-shaped beams and indicated that this method is more sensitive in case of low damping [23]. Worden compared the integration and differential of measured time data to construct the restoring force surface, and the influence of the selection of excitation signal on the identification of restoring force of linear and hardening spring oscillators was also illustrated [24,25]. Kerschen et al. utilized the restoring force surface method to identify the nonlinear beam with impact clearance and VTT benchmark system

based on acceleration-measurement [26,27]. Allen et al. proposed a piecewise-linear restoring force surface to identify the nonlinear electrostatic force of micro-cantilever beams based on velocity-measurement [28]. Noël et al. address the restoring force surface method companies with visual inspection and wavelet transform to a real-life aerospace structure with multiple mechanical stops and F16 aircraft wing-to-payload mounting interfaces [29,30]. Fuellekrug et al. studied the nonlinear stiffness force identification of a large transport aircraft under two coupled modes [31]. Moore et al. used acceleration-measurement to identify the nonlinear stiffness force in a grounded nonlinear energy sink system. The third-order Butterworth high-pass filter is employed to reduce the influence of low-frequency components in the integration procedure and the trend term [32]. The works mentioned above can be found that the restoring force surface method and its improved version can identify nonlinear restoring force without exact analytical expression in realistic structures. However, when considering the identification of strongly nonlinear structures, especially those working in low-frequency vibration environments or multi-stable properties, the previous acceleration and velocity-measurement restoring force surface method will encounter the problem that low-frequency components in integration procedure and complex trend items removing. Besides, for flexible structures such as cantilever beam systems, the influence of the size and mass of additional acceleration sensors attached to the system must be considered carefully. Most importantly, with the increasing use of strongly nonlinear structures in energy harvesting and vibration control, it is necessary to compare displacement-differentiation and acceleration-integration methods for constructing the restoring force surface and identifying nonlinearities in strongly nonlinear structures.

Therefore, the displacement-measurement restoring force surface approach is adopted in this paper to identify strongly nonlinear structures, and also a comparison with the acceleration-measurement restoring force surface method is discussed. To design a test rig for accurate verification, quasi-zero stiffness, bistable and tristable structures are conducted on a geometrically nonlinear cantilever beam with magnetic coupling. Based on the derived nonlinear model of the designed strongly nonlinear cantilever beam, the displacement-measurement restoring force surface identification method is adopted to obtain the nonlinear

stiffness and damping force. The influence of noise intensity on identification accuracy is also illustrated. Moreover, experimental measurements of quasi-zero stiffness, bistable and tristable nonlinear structures with various geometrical parameters are performed to comparatively analyze the identified nonlinear stiffness force and measured force-displacement trajectory. Experimental results verify the effectiveness of the proposed method.

The paper is organized as follows. In Section 2, the modeling theory of geometrically nonlinear cantilever beam is derived. The displacement-measurement restoring force surface identification process and comparison with acceleration-measurement restoring force surface method will be explained in detail in Section 3. Section 4 is dedicated to the numerical investigation and comparison of the proposed method, and further experimental verification and evaluation can be found in Section 5. Finally, the essential conclusions of the present study are summarized in Section 6.

2. Modeling of strongly nonlinear structures

A horizontal cantilever beam with rotatable magnetic coupling is designed in **Fig. 1(a)** to understand the dynamics of strongly nonlinear structures. The beam of length L carries two concentrated tip magnets C and the mass is M_m. Magnets C is subjected to two rotatable magnets A and B, arranged opposite magnets C. By changing the magnets' interval or rotatable angles, the cantilever beam will exhibit various nonlinear characteristics [9,10]. In this paper, only the quasi-zero stiffness, bistable and tristable beams are considered. **Fig. 1(b)** shows the quasi-zero stiffness beam under large deformation. The horizontal and vertical elastic displacements at the tip mass are x and y, respectively, and s represents the distance along the neutral axis of the beam. When considering an arbitrary point on the beam, p, at a distance s from the base, the laser displacement sensor can measure the response x_p of the point. In **Fig. 1(c)** and **Fig. 1(d)**，the bistable and tristable cantilever beams are illustrated. The bistable beam has two stable positions and one unstable position, while the tristable beam has three stable positions and two unstable positions.

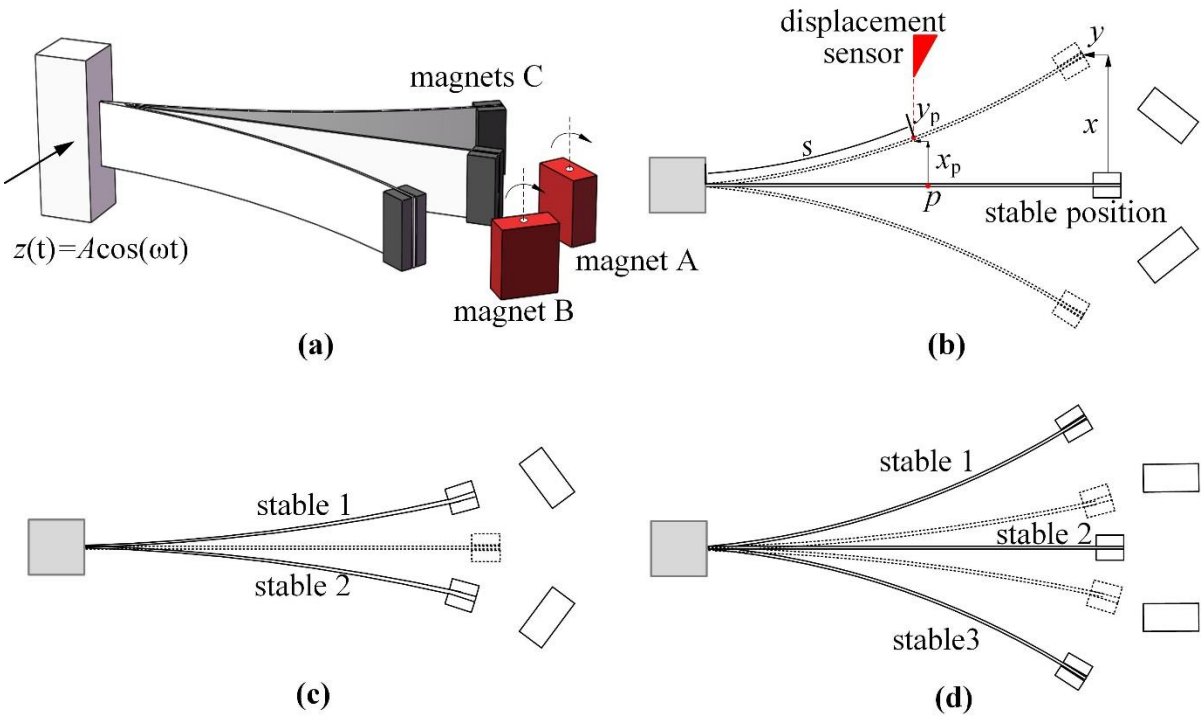

Figure. 1. (a) Schematic representation of magnetically coupled geometrically nonlinear cantilever beam with base excitation $z(t)=A\cos(\omega t)$; (b) quasi-zero stiffness beam. x and y denote the horizontal and vertical displacements of the tip magnets C respectively. Arbitrary point p on the beam whose position is described by the coordinates x_p, y_p and s; (c) bistable beam; (d) tristable beam.

In this section, the governing equation of motion will be derived by using the nonlinear Euler-Bernoulli beam theory and Lagrange's equation. It is assumed that the effects of shear deformation and rotary inertia of the beam can be neglected. Moreover, the effects of high order modes are much higher than the excitation frequency, and only the first-order mode needs to be considered. The beam has mass density ρ, cross-sectional area A, equivalent to Young's modulus E and second moment of inertia I. Neglecting the effect of rotary inertia of the beam and magnetic mass, the kinetic energy of the geometrically nonlinear beam-mass system is [33]:

$$T = \frac{1}{2}\rho A\int_0^L \left[(\dot{x}_p(s,t)+\dot{z})^2 + (\dot{y}_p(s,t))^2\right]ds + \frac{1}{2}M_m[(\dot{x}_p(L,t)+\dot{z})^2 + (\dot{y}_p(L,t))^2] \tag{1}$$

The elastic potential energy of the cantilever beam is:

$$U_e = \frac{1}{2}EI\int_0^L (\kappa(s,t))^2 ds \tag{2}$$

For magnetically coupled nonlinear structures, magnetic potential energy can be expressed as a polynomial model:

$$U_m = \sum_{n=1}^{q} \frac{1}{2} k_n (x)^n \tag{3}$$

where q denotes the order of polynomial functions and k is the coefficient. The relationship between curvature and slope of the beam is

$$\kappa(s,t) = \varphi_p' \tag{4}$$

The slope of the beam φ_p may be written in terms of the beam elastic displacement as

$$\cos\varphi_p = 1 - y_p' \text{ or } \sin\varphi_p = x_p' \tag{5}$$

Hence

$$\varphi_p(s,t) = \sin^{-1} x_p' \approx x_p' + \frac{1}{6} x_p'^3 \tag{6}$$

$$y_p' = 1 - \sqrt{1 - x_p'^2} \approx \frac{1}{2} x_p'^2 \text{ or } y_p(s,t) = \frac{1}{2}\int_0^s (x_p'(\xi,t))^2 d\xi \tag{7}$$

The differentiation of Eq. (6) can be described by

$$\kappa(s,t) \approx x_p''(1 + \frac{1}{2} x_p'^2) \tag{8}$$

The displacement at any point p can be represented as a function of the mass tip displacement through modal shape function, $\psi(s)$, as

$$x_p(s,t) = x_p(L,t)\psi(s) = x(t)\psi(s) \tag{9}$$

The displacement may be approximated by any function satisfying the boundary conditions at $s = 0$, for example:

$$\psi(s) = \lambda_t(1 - \cos(\frac{\pi s}{2L})) = \frac{1}{1 - \cos(\frac{\pi L_t}{2L})}(1 - \cos(\frac{\pi s}{2L})) \tag{10}$$

Based on the above analysis, the kinetic energy of the system in terms of the transverse displacement of the tip mass, x, are described as

$$\begin{aligned} T &= \frac{1}{2}\rho A\int_0^L \left[(\dot{x}\psi(s) + \dot{z})^2 + (x\dot{x}\int_0^s (\psi'(\xi))^2 d\xi)^2 \right] ds \\ &+ \frac{1}{2} M_m[(\dot{x} + \dot{z})^2 + (x\dot{x}\int_0^{L_t} (\psi'(s))^2 ds)^2] \\ &= \frac{1}{2}\rho A[N_1\dot{x}^2 + 2N_2 x\dot{x}\dot{z} + \dot{z}^2 L + N_3(x\dot{x})^2] + \frac{1}{2} M_m[(\dot{x} + \dot{z})^2 + N_4{}^2(x\dot{x})^2] \end{aligned} \tag{11}$$

and the total potential energy is

$$U = \frac{1}{2} EI \int_0^L \left[x\psi(s)'' + \frac{1}{2} x^3 (\psi'(s))^2 \psi''(s) \right]^2 ds + \frac{1}{2} \sum_{n=1}^{q} k_n (x_p(L,t))^n$$
$$= \frac{1}{2} EI [N_5 x^2 + N_6 x^4 + \frac{1}{4} N_7 x^6] + \frac{1}{2} \sum_{n=1}^{q} k_n (x)^n \tag{12}$$

the constants from N_1 to N_7 are given by

$$N_1 = \int_0^L \psi(s)^2 ds = \lambda_t^2 \left(\frac{3\pi - 8}{2\pi} \right) L;$$
$$N_2 = \int_0^L \psi(s) ds = \lambda_t \left(\frac{\pi - 2}{\pi} \right) L;$$
$$N_3 = \int_0^L \left(\int_0^s (\psi'(\xi))^2 d\xi \right)^2 ds = \lambda_t^2 \left(\frac{\pi^2 (2\pi^2 - 9)}{384} \right) \frac{1}{L};$$
$$N_4 = \int_0^{L_t} (\psi'(s))^2 ds = \lambda_t^2 \left(\frac{\pi^2}{8} \right) \frac{1}{L_t};$$
$$N_5 = \int_0^L (\psi''(s))^2 ds = \lambda_t^2 \left(\frac{\pi^4}{2^5} \right) \frac{1}{L^3};$$
$$N_6 = \int_0^L (\psi'(s)\psi''(s))^2 ds = \lambda_t^4 \left(\frac{\pi^6}{2^9} \right) \frac{1}{L^5};$$
$$N_7 = \int_0^L (\psi'(s)^4 \psi''(s))^2 ds = \lambda_t^6 \left(\frac{\pi^8}{2^{12}} \right) \frac{1}{L^7};$$

To obtain the motion equations of the proposed system, Lagrange's equation is defined as

$$\Gamma = T - U = \frac{1}{2} \rho A [N_1 \dot{x}^2 + 2N_2 \dot{x}\dot{z} + \dot{z}^2 L + N_3 (x\dot{x})^2]$$
$$+ \frac{1}{2} M_m [\dot{x}^2 + N_4{}^2 (x\dot{x})^2] - \frac{1}{2} EI [N_5 x^2 + N_6 x^4 + \frac{1}{4} N_7 x^6] - \frac{1}{n} \sum_{n=2}^{q} k_{n-1} x^n \tag{14}$$
$$\frac{d}{dt} \left(\frac{\partial \Gamma}{\partial \dot{x}} \right) - \frac{\partial \Gamma}{\partial x} = Q(t)$$

where Q(t) represents a generalized force, linear viscous damping force will be considered in any part of the beam.

$$Q(t) = -\int_0^L (c\dot{x}_p(s,t)) ds = -\int_0^L (c\dot{x}\psi(s)) ds = -N_2 c\dot{x} \tag{15}$$

Finally, the final equation of motion of the magnetically coupled nonlinear cantilever beam is obtained as

$$
\begin{aligned}
&(N_1\rho A + N_3\rho A x^2 + M_m + N_4{}^2 M_m x^2)\ddot{x} \\
&+N_2 c\dot{x} + (N_3\rho A + N_4{}^2 M_m)x\dot{x}^2 \\
&+N_5 EIx + 2N_6 EIx^3 + \frac{3}{4}N_7 EIx^5 + \sum_{n=2}^{q} k_{n-1}x^{n-1} \\
&= -(\rho A N_2 + M_m)\ddot{z}
\end{aligned}
\tag{16}
$$

It can be easily found from Eq. (16) that both the inertia force, damping force and stiffness force are nonlinear. However, the order of magnitude $(N_3\rho A+N_4{}^2M_m)x^2$ term in inertia force is relatively small. In many energy harvesting and vibration isolation structures, the deformation of the beam is not so large. So, the $(N_3\rho A+N_4{}^2M_m)x^2$ term will be neglected in the following sections.

3. Displacement-measurement restoring force surface method

The restoring force surface method in the time domain plots the internal restoring force of a nonlinear element as a function of displacement and velocity amplitudes. In this way, nonlinear stiffness and damping forces can be visualized by cutting the restoring force surface with a vertical plane where either the velocity or displacement is around zero, respectively. Theoretically, it is better to measure displacement, velocity and acceleration at each sampling point simultaneously. In practice, measuring the acceleration and then making an integration procedure to obtain the other two variables is common. Not all strongly nonlinear structures can construct the restoring force surface by measuring the acceleration and then extracting the nonlinear restoring force. The bistable or tristable structures presented in this paper may be an excellent example to prove it.

The specific process of restoring force surface construction and nonlinear stiffness extraction procedure will be shown as follows.

The Eq. (16) can be rearranged as

$$
\begin{aligned}
&f_{non}(x,\dot{x}) = f_c(x,\dot{x}) + f_k(x) = \\
&N_2 c\dot{x} + (N_3\rho A + N_4{}^2 M_m)x\dot{x}^2 + N_5 EIx \\
&+2N_6 EIx^3 + \frac{3}{4}N_7 EIx^5 + \sum_{n=2}^{q} k_{n-1}x^{n-1} \\
&= -(\rho A N_2 + M_m)\ddot{z} - (N_1\rho A + M_m)\ddot{x}
\end{aligned}
\tag{17}
$$

where $f_{non}(x,\dot{x})$ is excitation force minus inertia force, and also equal to the sum of damping force $f_c(x,\dot{x})$ and nonlinear stiffness force $f_k(x)$.

In Sec. 2, a displacement sensor was arranged at the position *p*, so the tip displacement can

be calculated using the modal shape function. Then, taking the three-point numerical differentiation program in Eq. (18), the velocity and acceleration will finally be obtained.

$$\dot{x}_u = \frac{-3x_{u-1} + 4x_u - x_{u+1}}{2dt};\ \ddot{x}_u = \frac{-3\dot{x}_{u-1} + 4\dot{x}_u - \dot{x}_{u+1}}{2dt} \tag{18}$$

where u denotes the location of the sampling point, and dt is the time interval.

It should be noted that the response trajectory of oscillators needs to cover the phase space as much as possible to provide enough and continuous data sets [24,25]. Therefore, the choice of the excitation source should be careful, especially for multi-stable structures. From the above procedure, the restoring force surface can be defined by the triplets $(x, \dot{x}, f_{non}(x, \dot{x}))$. Generally, cross sections of the restoring force surface along the axes where velocity and displacement are equal to zero yield nonlinear stiffness force curves and damping force curves, respectively.

However, it will lead to a failure or cause loss of identification accuracy if the sampling data around zero velocity is not sufficient for characterization. So, a more superior approach will be presented, and the detailed process of mathematical explanation is as follows.

The proposed restoring force surface can be expressed by a two-dimensional polynomial mathematical model as

$$f_{non}(x, \dot{x}) = \sum_{i=0}^{m}\sum_{j=0}^{n} \alpha_{ij} x^i \dot{x}^j \tag{19}$$

where m, n are the order of displacement x and velocity $\dot{x}$, respectively, and the coefficients α_{ij} can be obtained by the least square method. An essential procedure in the displacement-measurement restoring force surface method is cutting the restoring force surface with two vertical planes around zero velocity instead of using the one zero-velocity plane. It means the velocity range is chosen to $|\dot{x}| \le \delta_1$, δ_1 represents the distance between two vertical planes. Finally, projecting all the data sets $(x, \dot{x}, f_{non}(x, \dot{x}))$ to the zero-velocity plane, and the nonlinear stiffness force can be expressed as

$$f_k(x) = \sum_{i=0}^{m} k_i x^i \tag{20}$$

The k_i can be estimated by the least square method.

It can be observed in Eq. (17), the damping force becomes linear when the displacement is close to zero. So, another two vertical planes around zero displacements are adopted to cut the restoring surface. The interval between the two planes is selected as $|x| \le \delta_2$. Finally, projecting all the data sets $(x, \dot{x}, f_{non}(x, \dot{x}))$ to the zero-displacement plane, and the linear

damping force can be expressed as

$$f_c(\dot{x}) = \sum_{j=0}^{n} c\dot{x}^j \tag{21}$$

Least-squares parameter estimation can be utilized to obtain the values of the damping coefficients c.

To establish an evaluation standard between the identified value $f_k(x)$ and the theoretical one, the Normalised Mean-Square Error (NMSE) indicator is defined as [27]

$$NMSE(\hat{f}_{non}) = \frac{100}{N\sigma_{f_{non}}^2} \sum_{i=1}^{N} \left(f_{non} - \hat{f}_i \right)^2 \tag{22}$$

where $\sigma_{f_{non}^2}$ is the variance of the measured restoring force data sets and N is the total number of samples. The NMSE value of lower than 5% means good agreement while a value of less than 1% indicates a perfect fit. The error evaluation of the damping coefficient can be more accessible, and the relative error can be used directly.

The flow chart of identifying strongly nonlinear structures based on displacement-measurement restoring force surface method and some comparisons are shown in **Fig. 2**. It should be noted that the limitation of the displacement differential process will lead to the amplification of noise in the resulting velocity and accelerations. In this paper, the swept-frequency excitation is chosen, and a bandpass filter is adopted to solve this problem. When the velocity and acceleration are measured, there are two challenges in the integration procedure. Firstly, small low-frequency components in the acceleration data will be amplified relative to the components of interests. Though higher pass filtering can solve the problem, many strongly nonlinear structures work in low-frequency vibration conditions. Moreover, for multi-stable structures, the dynamic response must contains both inter-well and intra-well oscillation that allows construct the restoring force surface with the complete phase plane. However, by using the method of velocity integration, it is impossible to recognize the location of the oscillator oscillating any steady-state equilibrium points. The following sections of numerical investigation on bistable structures will give a specific explanation. Thus, for strongly nonlinear structures, especially quasi-zero stiffness and multi-stable structures, the displacement-measurement restoring force surface approach will be conducted and analyzed in more detail.

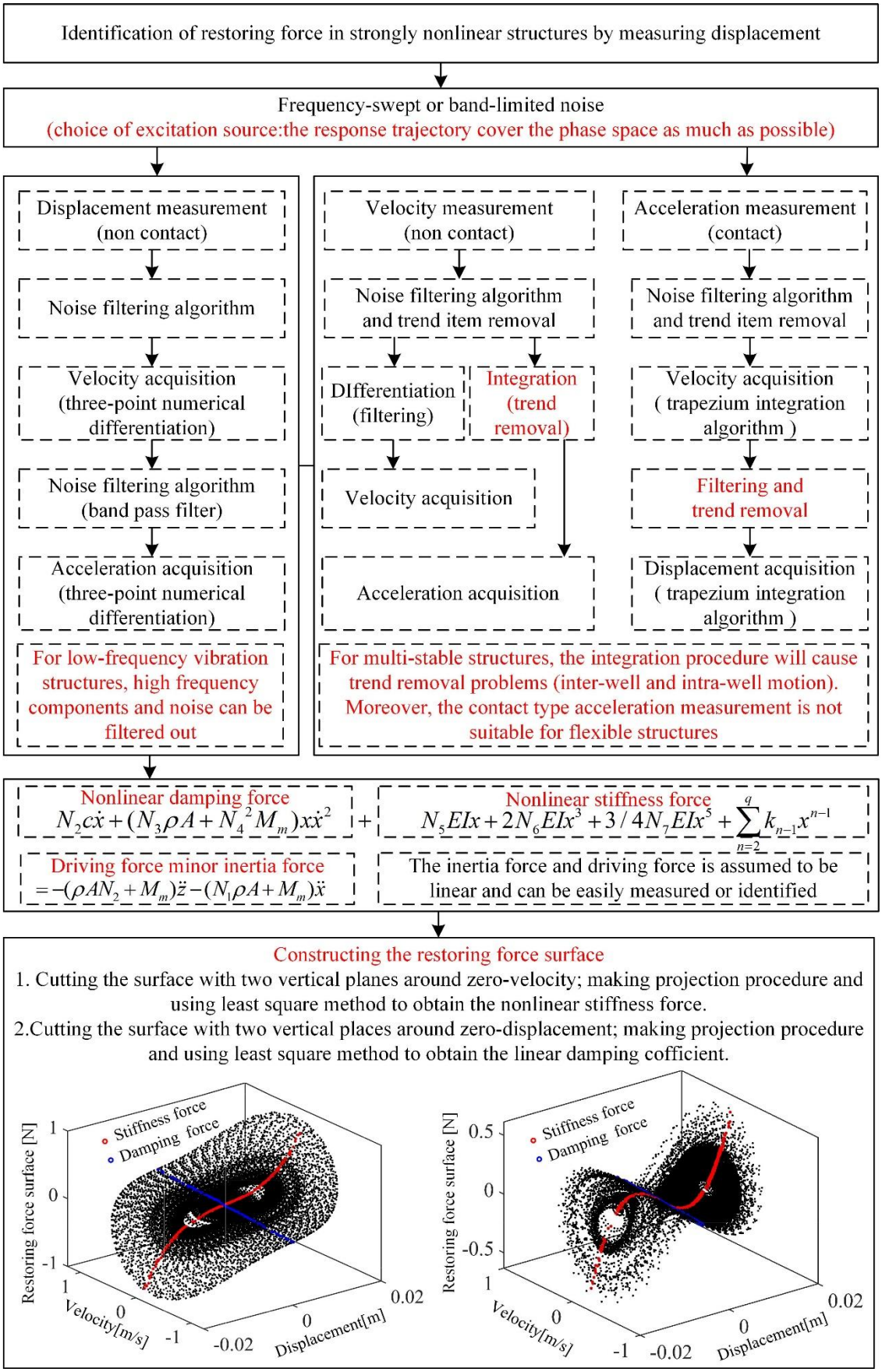

Figure. 2. A schematic diagram of the proposed displacement-measurement restoring force surface method for identification of nonlinear stiffness force and linear damping force in strongly nonlinear structures.

4. Numerical investigations

In this section, quasi-zero stiffness and bistable stiffness structures are illustrated for identification verification of the displacement-measurement restoring force surface method. The comparison between displacement-measurement and acceleration-measurement restoring force surface is conducted. Moreover, the influence of noise level on nonlinear restoring force identification accuracy is discussed.

The selection and calculation of the fundamental physical parameters of the beam are shown in **Table 1**. The physical meaning represented by the symbols had been described in **Sec. 2**.

Table 1. Parameters used in numerical simulations

Symbol	Numerical values	Symbol	Numerical values	Symbol	Numerical values
E	1.98×10^{11}N/m^2	M_m	4.2g	N_4	8.2247
L	0.15m	c	1N/(m/s)	N_5	901.936
b	0.01m	N_1	0.034	N_6	24727
h	0.0008m	N_2	0.0545	N_7	1.356×10^6
ρ	7810kg/m^3	N_3	1.8401		

In **Fig. 3**, the nonlinear stiffness force characteristics of the above-mentioned nonlinear structures are introduced. The quasi-zero stiffness with the function of $f_{non}=10x+10^5x^3+10^8x^5$ is shown in **Fig. 3(a)**. The stiffness is close to zero when the beam's deformation is small, and with the increase of deformation, the hardening characteristics will exhibit. For bistable stiffness structures with nonlinear stiffness force function of $f_{non}=-30x+3\times10^5x^3-10^8x^5$ is shown in **Fig. 3(b)**, three zero stiffness force points and one negative stiffness zone can be observed**.** The bistable characteristics will lead to inter-well and intra-well oscillation dependent on excitation level and will bring some difficulties in constructing the restoring force surface.

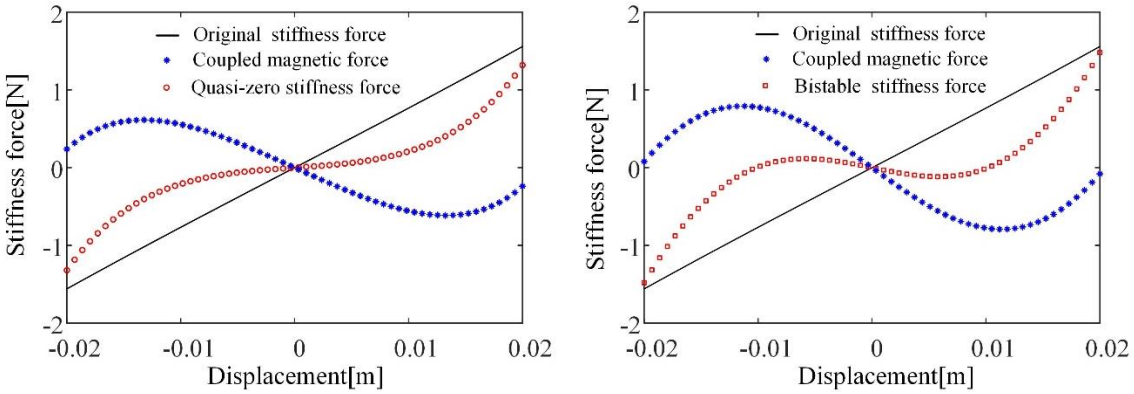

Figure. 3. Two types of nonlinear stiffness force: (a) Quasi-zero stiffness structures; (b) bistable structures.

4.1 Comparison between differentiation and integration

An 80-second forward sine sweep followed by a backward sine sweep signal is conducted on the system to excite the quasi-zero stiffness system. The sampling frequency is 500Hz, and the frequency range is 0~20Hz. The classic fourth-order Runge-Kutta is adopted to solve the second-order differential equation. **In Fig. 4(a)**, the blue line shows the complete time-domain displacement response of the oscillator. And then, a 50 Hz Butterworth low pass filter and a three-point numerical differentiation algorithm are conducted. After one and two times of this process, both the velocity (red line) and acceleration(green line) response can be obtained. The resulting data sets of displacement, velocity and acceleration are substituted into Eq. (17), and then the restoring force surface was constructed as depicted in **Fig. 4(b)**. Meanwhile, two vertical zero-velocity planes with δ_1=0.02 were selected to cutting the restoring force surface, and the red circle line shows the intercepted trajectories. Besides, the blue circle represents the intercepted trajectories obtained by using two vertical zero-displacement planes with δ_2=0.0002. **Fig. 4(c)** shows the comparison between the identified nonlinear stiffness force and the theoretical one. The NMSE error is 0.041%, which indicates a perfect fit. In **Fig. 4(d)**, the identified linear damping force trajectories do not match as well with the theoretical one because small assumed displacement cutting planes will cause upper and lower deviation of intercepted nonlinear damping force data sets. The final relative error is 8.26%. For the same quasi-zero stiffness oscillator with the same excitation source, an integration procedure from the acceleration time-domain sequence was also conducted. **Fig. 4(e)** presents the acceleration response (green line), and the trapezium integration and the second-order trend term removal algorithm was adopted to obtain the velocity (red line) and displacement (blue line). In **Fig. 4(f),** the acceleration-measurement restoring force surface was constructed and the nonlinear stiffness force and damping force trajectories are extracted. It can be observed in **Fig. 4(g)** that the identified nonlinear restoring force error is only 0.087%. But, the identified damping force still has a poorly fitting and the relative error reaches 11.93%, as shown in **Fig. 4(h)**. The above results reveal that for monostable quasi-zero stiffness structures, both displacement-measurement and acceleration-measurement methods for constructing the restoring force surface can identify the nonlinear stiffness force well. For damping coefficient identification, both methods need to be used with caution because of relatively higher error.

For bistable structures, it can exhibit both inter-well or intra-well motions dependent on the excitation and the initial conditions. Based on the contribution of Wooden [24,25], the excitation source must make the response trajectory cover the phase plane as much as possible.

If the bistable structure oscillating completely across the potential well or only make intra-well motions, it is impossible to construct the good restoring force surface or make the lousy fitting accuracy. In this example, a forward sine sweep followed by a backward sweep with the frequency range of 5~25Hz is adopted. The swept time is 80s with a sampling frequency 500Hz. **Fig. 5(a)** shows the displacement, velocity and acceleration responses of the oscillator. The 5~50Hz Butterworth bandpass filtering program and differential procedure are conducted for obtaining the velocity and acceleration sequence. In **Fig. 5(b)**, the restoring force surface is constructed and the intercepted nonlinear stiffness force and damping force are marked by red and blue circles, respectively. In **Fig. 5(c)**, the identified nonlinear stiffness force fitted well with the theoretical curve and the NMSE error is only 0.093%. The identified damping force shown in **Fig. 5(d)** still has low accuracy. From the above mentioned, the displacement-measurement restoring force surface method can identify the nonlinear restoring force well in bistable structures, especially the nonlinear stiffness force. In **Fig. 5(e)**, the acceleration response sequence is presented first and then make integration procedure. Finally, the velocity and displacement sequence are given. It can be observed from **Fig. 5(f)** that the displacement to velocity integration procedure is reasonable, but the integrated displacement based on velocity is wrong as shown in **Fig. 5(g)**. Many trend term removal methods such as mean removal, second-order trend removal, and highpass filter are adopted for obtaining the reasonable displacement response but failed to run. It's a great difficulty to make the integration and detrended program to locating the inter-well and intra-well motion in the dynamic response of bistable oscillators. It can be observed in **Fig. 5(h)** that the constructed restoring force surface data sets are wrong and the following nonlinear restoring force extraction process can not be completed.

From the above numerical analysis, it can be found that the displacement-measurement restoring force surface method may be more desirable for the identification of quasi-zero and bistable structures. So, it is necessary to start from the time series of displacement measurement to make identification procedures in bistable structures. However, measuring the displacement and then differentiating leads to the noise amplification in the resulting velocity and accelerations. In the next section, the influence of noise level on the identification accuracy of nonlinear stiffness force will be discussed. The damping force will not be discussed here because no noise pollution in the identification process had already lead to more significant errors.

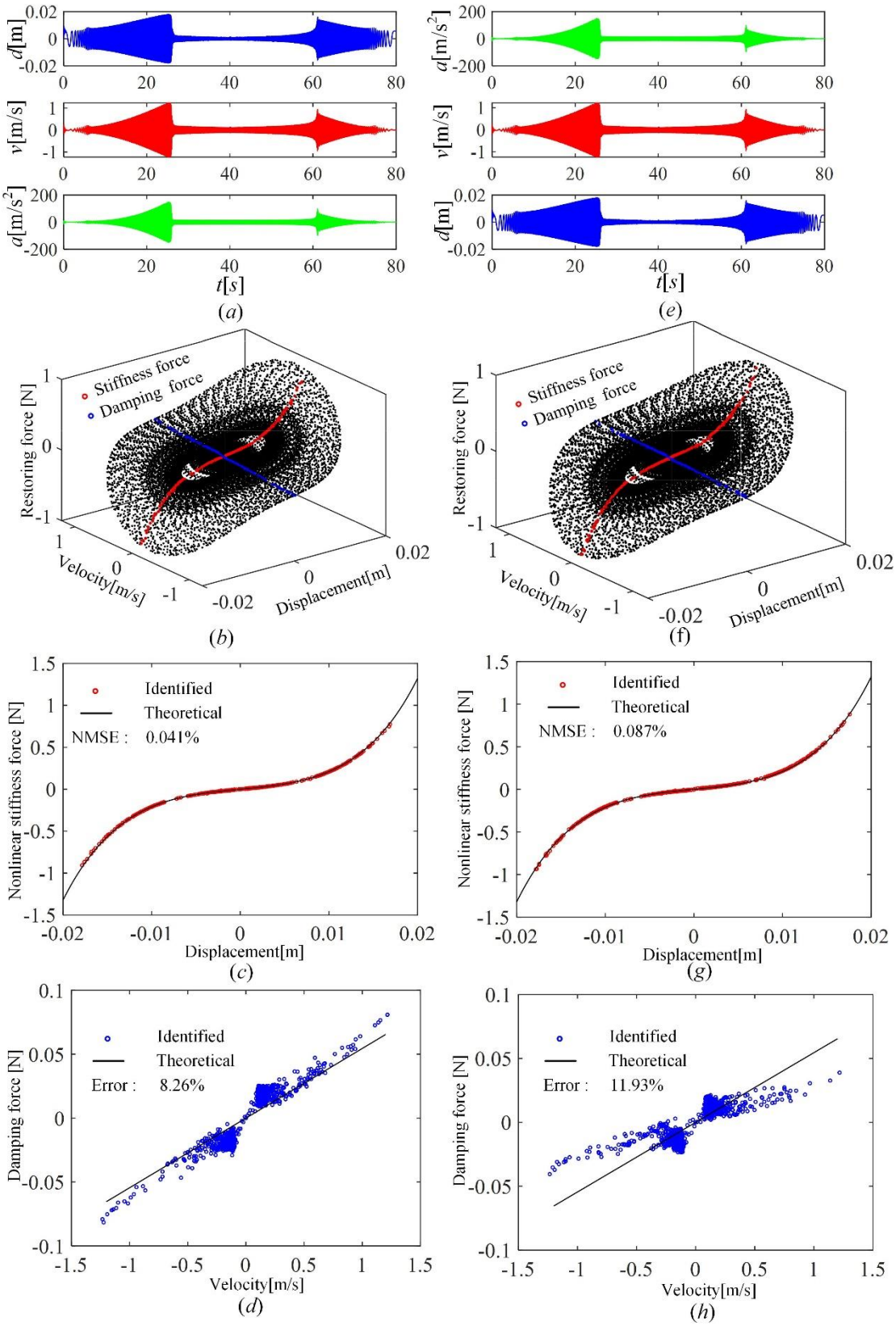

Fig. 4 Comparison between displacement-measurement and acceleration-measurement restoring force surface for identification of quasi-zero stiffness structures: (a) differentiation procedure; (b) restoring force surface; (c) nonlinear stiffness force identification and NMSE error; (d) nonlinear damping identification and relative error of damping coefficient. (e,f,g,h) integration procedure and the identification process.

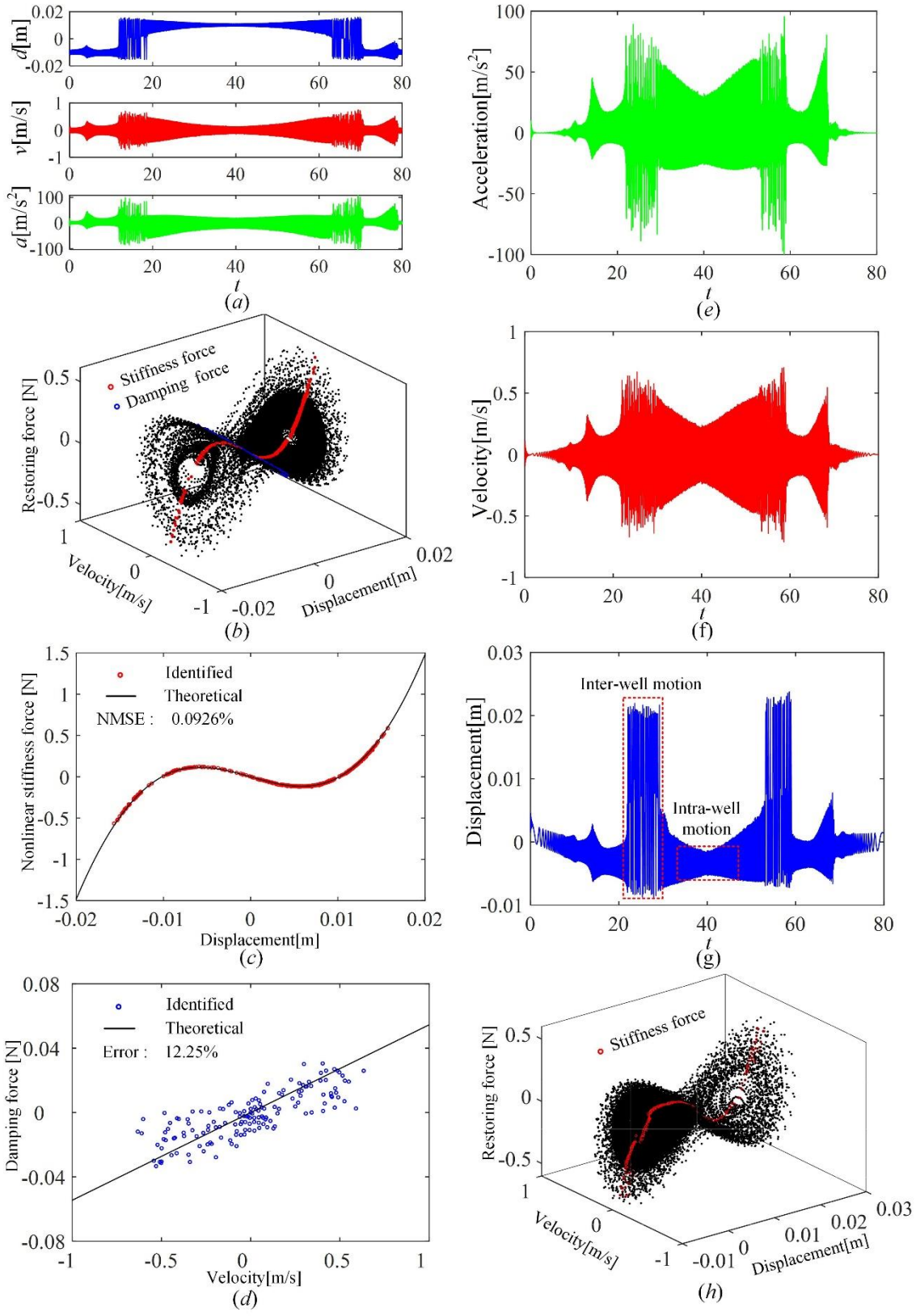

Fig. 5 Comparison between displacement-measurement and acceleration-measurement restoring force surface for identification of bistable structures: (a) differentiation procedure; (b) restoring force surface; (c) nonlinear stiffness force identification and NMSE error; (d) nonlinear damping identification and relative error of damping coefficient. (e,f,g,h) integration procedure and the identification process.

4.2 Influence of noise level on identification accuracy

In this section, the noise level on identification accuracy of nonlinear stiffness force in quasi-zero stiffness and bistable structures are discussed. The noise intensities of 40dB, 30dB and 20dB are added to the displacement response, respectively, and then make some comparisons.

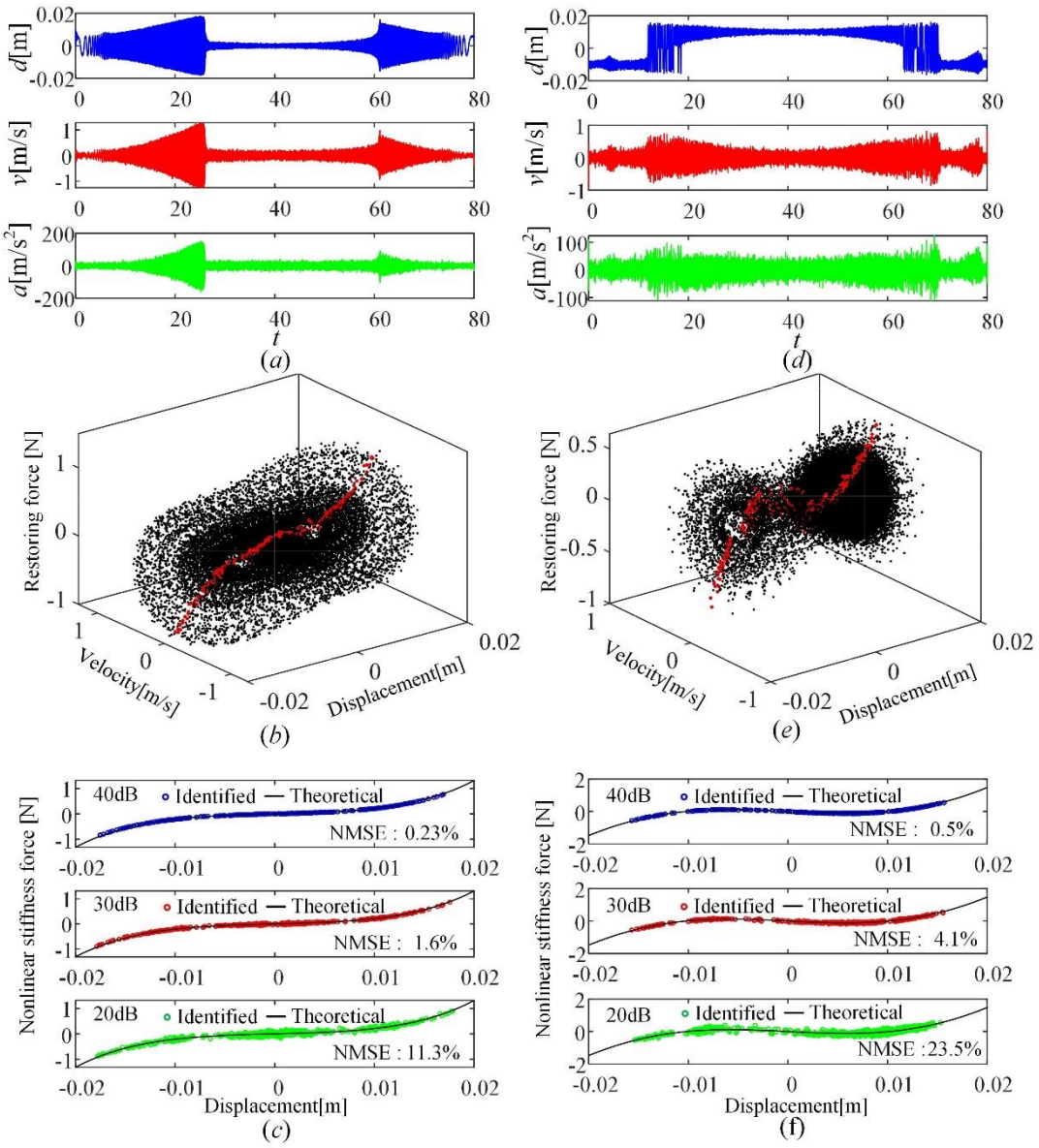

Fig. 6 The influence of noise level on identification accuracy of quasi-zero stiffness and bistable structures. (a) the frequency-swept displacement response of quasi-zero stiffness structures and the resulting velocity and acceleration based on filtering and differentiation program; (b) the constructed restoring force surface and the nonlinear stiffness force trajectory; (c) the identified nonlinear stiffness force compared with the theoretical one under the noise of 40dB, 30dB and 20dB respectively; (e,f,g) the dynamic response of the bistable system, constructed restoring force surface and the identified nonlinear stiffness force comparison.

In **Fig. 6(a)**, the frequency-swept displacement response with 20dB noise of quasi-zero

stiffness structures is shown, and then the same procedure in Sec. 4.1 is adopted for obtaining velocity and acceleration. **Fig. 6(b)** presents the constructed restoring force surface and intercepted nonlinear stiffness force data sets. In **Fig. 6(c)**, the identified nonlinear stiffness force with the noise level of 40dB, 30dB and 20dB are shown and the NMSE error are 0.23%, 1.6% and 11.3% respectively. With the increase of the noise level, the identification accuracy decreases, and identification results are close to real value when the noise level below 30dB. For bistable structures, the 40dB, 30dB and 20dB noise are also added to the frequency-swept displacement response. **Fig. 6(d)** presents the displacement response with 20dB noise, and the resulting velocity and acceleration by differentiation procedure are also given. In **Fig. 6(e)**, the constructed restoring force surface for the bistable oscillator is shown and the red circle line is the nonlinear stiffness force trajectory. The final identification results are plotted in **Fig. 6(f)**. Similarly, the identified nonlinear stiffness force can keep a good fit when the noise level is lower than 30dB. In general, the identification accuracy of bistable oscillators is lower than quasi-zero stiffness structures. Considering the inter-well and intra-well chaos motion is more complicated than the frequency-swept response in monostable structures, the lower accuracy in identifying bistable structures is reasonable.

5. Experimental validations

To verify the displacement-measurement restoring force surface method for nonlinear stiffness force identification of three strongly nonlinear structures in realistic conditions, an experimental test rig is set up in **Fig. 7(a)**. The quasi-zero stiffness, bistable stiffness and tristable stiffness structures are designed in the cantilever beam system with rotatable magnets coupling function. The excitation source is generated by a vibration exciter (JZK-50, Econ Technologies Co., Ltd), a power amplifier (YE5874A, Econ Technologies Co., Ltd), and a vibration controller (VT-9002-1, Econ Technologies Co., Ltd) is used to realize the feedback and real-time control of excitation signal. A displacement sensor (HL-G112-A-C5, Keyence) is applied to measure the relative displacement response and the data sets are collected by an oscilloscope (MSOX3052A, Agilent). Another acceleration sensor (EV4540, Econ Technologies Co., Ltd) is installed on the fixture to monitor the vibration exciter output signal and transmit it to the data acquisition instrument (MI-70080, Econ Technologies Co., Ltd).

In the experiments, the cantilever beam is made of 65Mn spring steel and has a dimension of $146.5\times10\times0.8mm^3$. All cantilever beams have two endmost magnets except for tristable beam 2 (low potential well tristable have four magnets). The magnet's size is $10\times10\times2.5mm^3$ and the property is NdFeB. To extract the continuous nonlinear stiffness force curve from the displacement-measurement restoring force surface method discussed in **Sec. 3**, the mode of forwarding sine swept-frequency followed with the same intensity of backward swept-frequency is adopted in the experimental excitation. More detailed parameters of the configuration of four typical beams and excitation level are illustrated in **Table 2**.

Table 2. Experimental excitation parameters for system identification

Types	Equilibrium position (mm)	Frequency range (Hz)	Excitation acceleration (m/s^2)
Quasi-zero stiffness	0	5~25	3.5
Bistable stiffness	-8.16 ; 0 ; 10.4	10~30	8
Tristable stiffness1	-11.4 ; -6.29 ; 0 ; 5.9 ; 13.4	10~30	10.5
Tristable stiffness2	-11 ; -6.7 ; 0 ; 8.2 ; 14.1	8~28	8

Another nonlinear stiffness force measurement experimental setup is shown in **Fig. 7(b)**. The Force Gauge (M5-2, MARK-10 Corporation) is installed on the structure driven by the ball screw and the resolution is 0.002N. As the dynamometer pushes the cantilever beam to deform, the movement displacement will be recorded by Digital Indicator. Each measurement needs to be carried out from the steady-state point position and then arrange the force-displacement data from negative to positive deflection. This means the number of measurements is divided into two, four and six segments for quasi-zero stiffness, asymmetric bistable and asymmetric tristable beams.

Moreover, the force gauge cannot be installed on the designed test fixture to identify the equivalent mass. So, the linear stiffness of the cantilever beam is measured firstly, and the value is K=80N/m, and then a swept-frequency excitation signal was conducted on the linear cantilever beam and the resonant frequency is 18.5Hz. By using the equation of $M=80/(18.5\times2\pi)^2$, the equivalent mass $M=5.9\times10^{-3}$kg.

It must be emphasized that the dynamic response needs to be reconstructed based on the identified nonlinear restoring force and then compared with the measured data sets [32-34].

Generally, it is necessary to do so to verify the accuracy of the results. However, for strongly nonlinear structures like the bistable system investigated in this paper, It is almost impossible to complete the task making the reconstruction response in good agreement with the actual acquisition response. The dynamic response of the bistable system is very sensitive to the nonlinear coefficients, initial conditions and excitation level, etc. So, the slightly incorrect identification results maybe cause the oscillator to exhibit different forms of chaos movement. In this paper, the identified nonlinear stiffness force is compared with the directly measured one. Besides, the nonlinear stiffness force of the actual magnetic coupling cantilever is not a perfect polynomial or a smooth spline, and it can not be accurately fitted. So, qualitative comparisons are considered in experimental investigations.

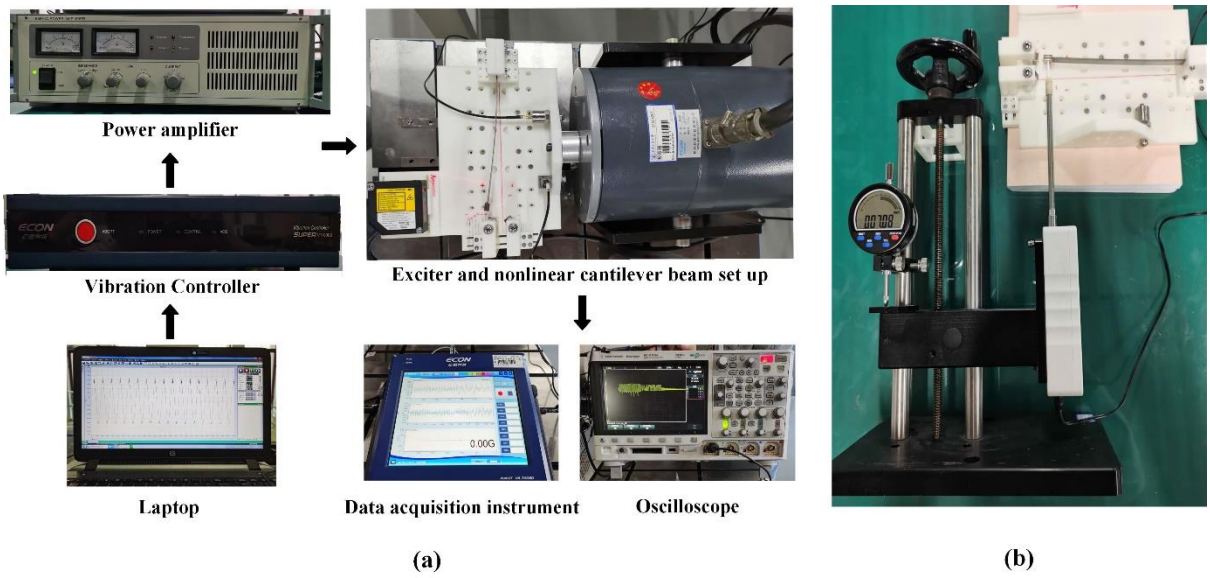

Figure. 7. Experimental set-up: (a) excitation generation, control and signal acquisition equipment; (b) nonlinear stiffness force measuring instrument.

Firstly, the displacement-measurement restoring force surface method is applied to quasi-zero stiffness and bistable cantilever beams. **Fig. 8** shows the whole process from displacement response to identified nonlinear stiffness force. In **Fig. 8(a),** the beam is excited by a forward sine sweep (5~25Hz) followed by a backward sine sweep (25~5Hz) with a sampling frequency of 500Hz at the constant acceleration of 3.5m/s^2. The jumping phenomenon is not as apparent as the quasi-zero stiffness beam in numerical investigations. **Fig. 8(b)** shows the constructed restoring force surface, and the nonlinear stiffness force curve remarked by the red circles are extracted by assuming the velocity $|\dot{x}| \leq 0.02$m/s. The extracted nonlinear stiffness force

curve is not monotonically increasing and both hardening and softening properties can be seen. This is because it is tough to construct a perfect zero stiffness zone around the steady-state point in real applications and a relatively close zero stiffness is achieved by coupling two negative stiffness regions. If the magnetic force keeps increasing and the nonlinear stiffness force crosses zero points, the bistable and tristable phenomenon will occur. In **Fig. 8(c)**, the identified nonlinear stiffness force curve and measured force-displacement trajectory was compared and show good consistency. **Fig. 8(d)** shows the bistable beam dynamic response under a forward sine sweep (10~30Hz) followed by a backward sine sweep (30~10Hz) with a sampling frequency of 500Hz at the constant acceleration of $8m/s^2$. This type of response is suitable for restoring force surface construction shown in **Fig. 8(e)** and the nonlinear stiffness force extraction is shown in **Fig. 8(f).** It can be observed from **Fig. 8(f)** that the nonlinear stiffness force identified by the proposed method is very reliable when compared to the measured force-displacement trajectory.

As for designing a multi-stable vibration structure or putting it into practical use, the potential wells and equilibrium points are critical factors [35,36]. For example, a tristable piezoelectric energy harvester needs to make a nonlinear stiffness force design based on the intensity and frequency range of environmental excitation. Moreover, the equilibrium points cannot be designed too large and this will cause piezoelectric layers to break up. Generally, it should be designed with low potential wells to work in a weak and low-frequency excitation environment.

To verify the ability of the displacement-measurement restoring force surface method for nonlinear stiffness force identification of different multi-stable structures, two asymmetric tristable beams with high potential wells and low potential wells are compared in **Fig. 9**. One noticeable feature is that the beam with high potential wells is hard to fully motivated, as shown in **Fig. 9(a)**, but as for low potential wells, the oscillator traveling across the potential wells in a large swept frequency range, as shown in **Fig. 9(b)**. However, a relatively good restoring force surface and nonlinear stiffness force data sets were constructed in high potential well tristable oscillator compared to the beam with low potential wells as shown in **Fig. 9(c)** and **Fig. 9(d).** It must be emphasized here that the tristable oscillator with low potential wells can also generate an excellent original displacement response for the displacement-measurement restoring force surface identification process. Numerous examples and experiments had been conducted in this paper, and only these two types were chosen to make a more intuitive comparison. Consequently, by comparing the identified results with the measured force-displacement trajectory in **Fig. 9(e)** and **Fig. 9(f)**, the proposed identification method has strong

applicability to multi-stable structures with different potential wells and equilibrium points.

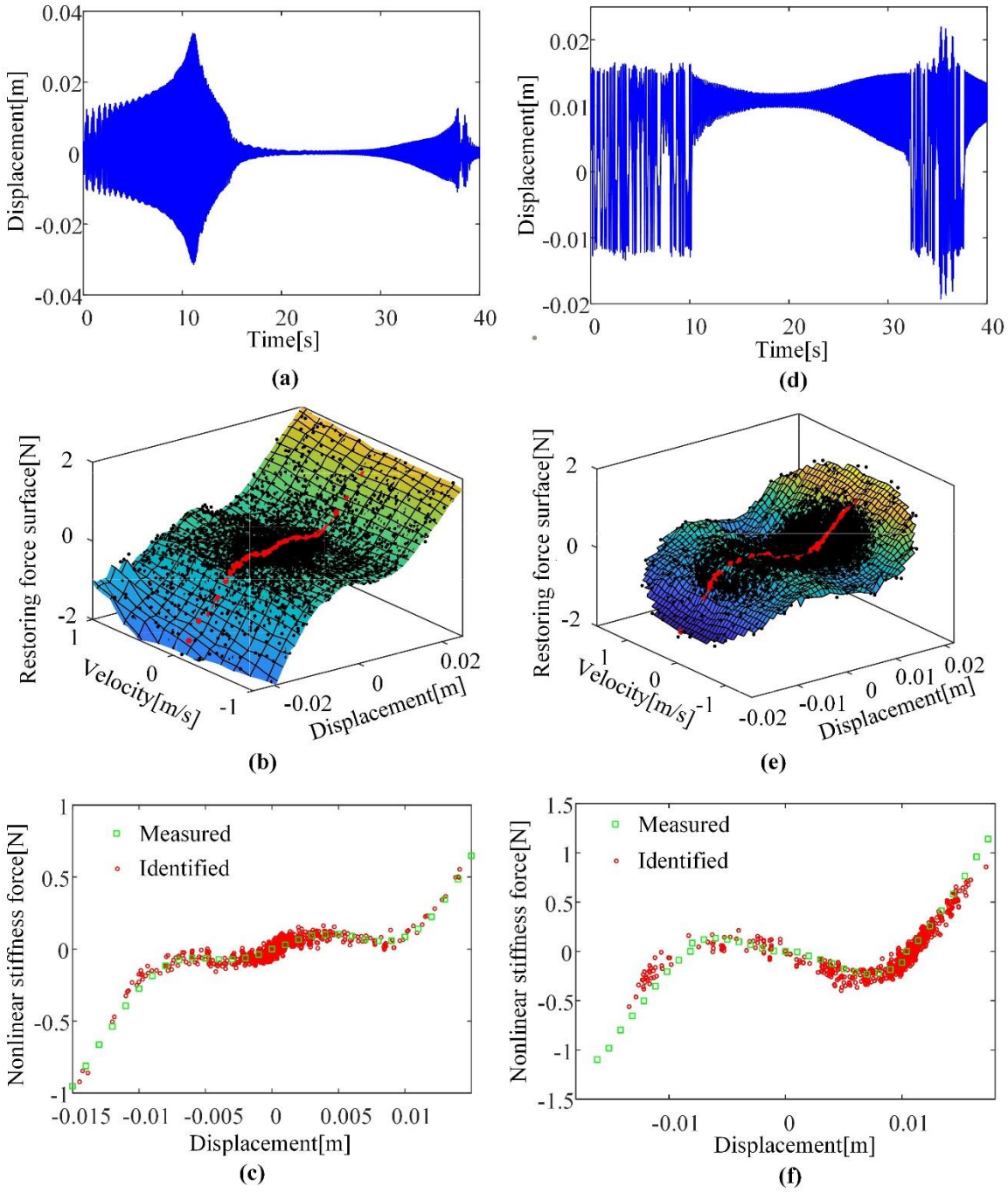

Fig. 8. (a,d) Frequency-swept response of the quasi-zero stiffness and bistable stiffness oscillator; (b,e) constructed restoring force surface and extracted nonlinear stiffness force curve by cutting the restoring force surface with two vertical zero-velocity planes; (c,f) comparison between identified and measured nonlinear stiffness force.

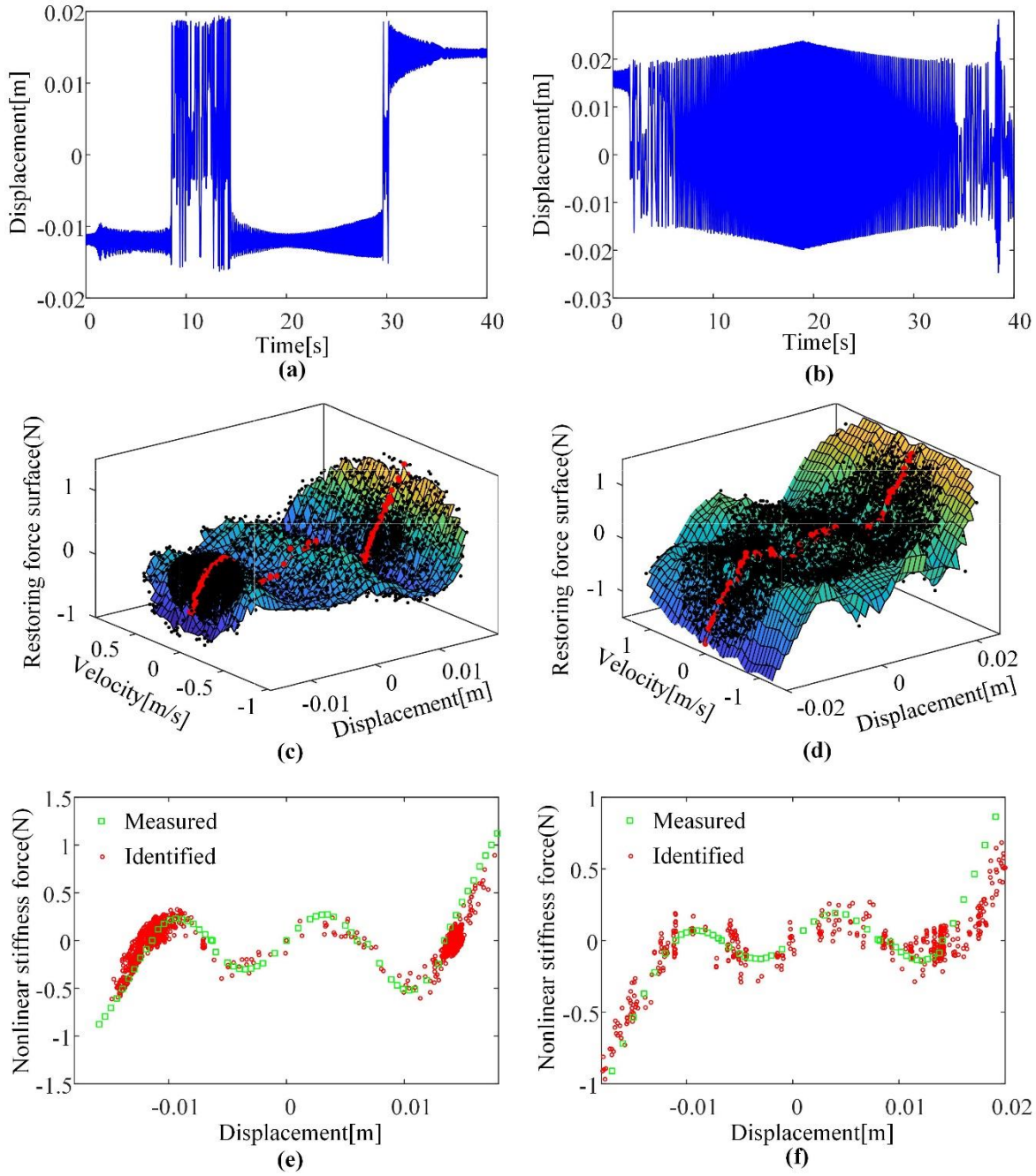

Fig. 9. (a,b) The swept-frequency response of tristable oscillators with high potential wells and low potential wells depth. (c,d) constructed restoring force surface and extracted nonlinear stiffness force; (e,f) comparison of identified nonlinear stiffness force curve and measured force-displacement trajectory.

6. Conclusions

This paper investigates the displacement-measurement restoring force surface method for the identification of nonlinear restoring force in strongly nonlinear structures. To verify the effectiveness and accuracy of the identification procedure, quasi-zero stiffness and bistable

structures are numerically investigated. By comparing with the acceleration-measurement restoring force surface method, it can be found that the method of measuring acceleration and make integration procedure cannot obtain the reasonable inter-well and intra-well displacement response in bistable systems. So, starting from the time series of displacement measurement to construct the restoring force surface for nonlinear restoring force identification is necessary. In monostable quasi-zero stiffness structures, though the acceleration-measurement method for identification is feasible, its accuracy is lower than that of the displacement-measurement approach. Besides, the displacement-measurement restoring force surface method is robust for identifying the nonlinear stiffness force in strongly nonlinear structures when the noise is lower than 30dB. In experimental conditions, the quasi-zero stiffness, bistable and tristable cantilever beam are designed to obtain their displacement response for identifying the restoring force. The identified nonlinear stiffness force curve has a good agreement with the directly measured force-displacement trajectory. Moreover, the identified results of two asymmetric tristable structures show that the displacement-measurement restoring force surface method has strong applicability for those multi-stable structures with different potential wells and equilibrium points.

Authorship contribution statement

Q.H. Liu: Conceptualization, Methodology, Software, Experimental Validation, Investigation, Writing - original draft. **Z.H. Hou:** Software, Investigation. **Y. Zhang:** Experimental Validation, Investigation. **X.J. Jing:** Supervision, Writing - review & editing. G. Kerschen: Conceptualization, Supervision, Writing - review & editing. **J.Y. CAO:** Conceptualization, Methodology, Supervision, Writing - review & editing.

Declaration of Competing Interest

The authors declare that they have no known competing financial interests or personal relationships that could have appeared to influence the work reported in this paper.

Acknowledgment

This work is sponsored by the National Natural Science Foundation of China (Grant no. 51975453)

References

[1] A. Carrella, M.J. Brennan, T.P. Waters, V.J. Lopes, Force and displacement transmissibility of a nonlinear isolator with high-static-low-dynamic-stiffness, Int. J. Mech. Sci. 55(2012) 22-29.

[2] D.L. Thanh, K.A. Kyoung, A vibration isolation system in low frequency excitation region using negative stiffness structure for vehicle seat, J. Sound Vib. 330(2011) 6311-6335.

[3] X.T. Sun, X.J. Jing, Multi-direction vibration isolation with quasi-zero stiffness by employing geometrical nonlinearity, Mech. Syst. Signal Process. 62-63(2015) 149-163.

[4] X.J. Jing, L.L. Zhang, G.Q. Jing, X. Feng, Y.Q. Guo, Z.D. Xu, Critical factors in designing a class of X-shaped structures for vibration isolation, Eng. Struct. 199(2019) 109659.

[5] J.X. Zhou, X.L.Wang, D.L. Xu, S. Bishop, Nonlinear dynamic characteristics of a quasi-zero stiffness vibration isolator with cam-roller-spring mechanisms, J. Sound Vib. 346(2015) 53-69.

[6] Y.H. Yao, H.G. Li, Y. Li, X.J. Wang, Analytical and experimental investigation of a high-static-low-dynamic stiffness isolator with cam-roller-spring mechanism, Int. J. Mech. Sci. 186(2020) 105888.

[7] J.T. Zhang, J. Zhang, C. Shu. Z. Fang, Enhanced piezoelectric wind energy harvesting based on a buckled beam, Appl. Phys. Lett. 110(2017) 3-468.

[8] X.T. Liu, X.C. Huang, H.X. Hua, On the characteristics of a quasi-zero stiffness isolator using Euler buckled beam as negative stiffness corrector, J. Sound Vib. 332(2013) 3359-3376.

[9] S.X. Zhou, J.Y. Cao, A. Erturk, J. Lin, Enhanced broadband piezoelectric energy harvesting using rotatable magnets, Appl. Phys. Lett. 102(2013) 101301-R21.

[10] J.Y. Cao, S.X. Zhou, W. Wang, J. Lin, Influence of potential well depth on nonlinear tristable energy harvesting, Appl. Phys. Lett. 106(2015) 515-530.

[11] X.J. Jing, L.L. Zhang, X. Feng, A.K. Li, A novel bio-inspired anti-vibration structure for operating hand-held jackhammers, Mech. Syst. Signal Process. 118(2019) 317-339.

[12] S.C. Stanton, C.C. McGehee, B.P. Mann, Nonlinear dynamics for broadband energy harvesting: Investigation of a bistable piezoelectric inertial generator, Physica D. 239(2010) 640–653.

[13] G.Q. Wang, Z.X. Zhao, W.H. Liao, J.P. Tan, Y, Ju, Y. Li, Characteristics of a tri-stable piezoelectric vibration

energy harvester by considering geometric nonlinearity and gravitation effects, Mech. Syst. Signal Process. 138(2020) 1-18.

[14] Y. Zhang, J.Y. Cao, W. Wang, W.H. Liao, Enhanced Modeling of Nonlinear Restoring force in multi-stable energy harvesters, J. Sound. Vib. 494(2020).

[15] S. Leadenham, A. Erturk, Nonlinear M-shaped broadband piezoelectric energy harvester for very low base accelerations: primary and secondary resonances, Smart Mater. Struct. 24(2015) 55021.

[16] J.P. Noël, G. Kerschen, Nonlinear system identification in structural dynamics: 10 more years of progress, Mech. Syst. Signal. Process. 83 (2017) 2-35.

[17] S. Marchesiello, L. Garibaldi, A time domain approach for identifying nonlinear vibrating structures by subspace methods, Mech. Syst. Signal. Process. 22(2008) 81-101.

[18] J.P. Noël, S. Marchesiello, G. Kerschen, Subspace-based identification of a nonlinear spacecraft in the time and frequency domains, Mech. Syst. Signal. Process. 43(2014) 217-236.

[19] G.D. Filippis, J.P. Noël, G. Kerschen, L. Soria, C. Stephan, Experimental nonlinear identification of an aircraft with bolted connections, IMAC, Orlando, FL (2014).

[20] J.P. Noël, G. Kerschen, Frequency-domain subspace identification of nonlinear mechanical systems - Application to a solar array structure. Mech. Syst. Signal. Process. 40(2013) 701-717.

[21] S.F. Masri, T.K. Caughey, A nonparametric identification technique for nonlinear dynamic problems, J. Appl. Mech. 46 (1979) 433–447.

[22] E.F. Crawley, A.C. Aubert, Identification of nonlinear structural elements by force-state mapping, AIAA J. 24 (1986) 155–162.

[23] M. A Al-Hadid, J.R. Wright, Application of the force-state mapping approach to the identification of non-linear systems, Mech. Syst. Signal. Process. 4 (1990) 463–482.

[24] K. Worden, Data processing and experiment design for the restoring force surface method, part I: integration and differentiation of measured time data, Mech. Syst. Signal. Process. 4 (1990) 295-319.

[25] K. Worden, Data processing and experiment design for the restoring force surface method, part II: Choice of excitation signal, Mech. Syst. Signal. Process. 4 (1990) 321-344.

[26] G. Kerschen, J.C. Golinval, Theoretical and experimental identification of a non-linear beam, J. Sound Vib. 244 (2001) 597–613.

[27] G. Kerschen, V. Lenaerts, J.C. Golinval, VTT benchmark: Application of the restoring force surface method, Mech. Syst. Signal. Process. 17(2003) 189-193.

[28] M.S. Allen, H. Sumali, and D.S. Epp, Piecewise-linear restoring force surfaces for semi-nonparametric identification of nonlinear systems, Nonlinear Dynam. 54(2008) 123-135.

[29] J.P. Noël, L. Renson, G. Kerschen, Complex dynamics of a nonlinear aerospace structure: Experimental identification and modal interactions, J. Sound Vib. 333(2014) 2588-2607.

[30] J.P. Noël, L. Renson, G. Kerschen, B. Peeters, S. Manzato, J. Debille, Nonlinear dynamic analysis of an F-16 aircraft using GVT data, in: Proceedings of the International Forum on Aeroelasticity and Structural Dynamics, 2013.

[31] U. Fuellekrug, D. Goege, Identification of weak non-linearities within complex aerospace structures, Aerosp. Sci. Technol. 23(2012) 53-62.

[32] K.J. Moore, M. Kurt, M. Eriten, D.M. McFarland, L.A. Bergman, A.F. Vakakis, Time-series based nonlinear system identification of modal interactions caused by strongly nonlinear attachments, J. Sound Vib. 438 (2019) 13–32.

[33] M.I. Friswell, S.F. Ali, O. Bilgen, S. Adhikari, W.L. Arthur, G. Litak, Non-Linear piezoelectric vibration energy harvesting from a vertical cantilever beam with tip mass, J. Intel. Mat. Syst. Str. 23(2013) 1505-1521.

[34] M. Feldman, Nonparametric identification of asymmetric nonlinear vibration systems with the Hilbert transform, J. Sound Vib. 331(2012) 3386-3396.

[35] T.C. Yuan, J. Yang, L.Q. Chen, Nonparametric Identification of Nonlinear Piezoelectric Mechanical Systems, J. Appl. Mech. 85(2018) 111008.

[36] B. Xu, J. He, S.F. Masri, Data-based Identification of nonlinear restoring force under spatially incomplete excitations with power series polynomial model, Nonlinear Dynam. 67(2012) 2063-2080.

[37] Huang D, Zhou S , Li W, G. Litak, On the stochastic response regimes of a tristable viscoelastic isolation system under delayed feedback control. Sci China Technol Sc. 4(2020).

[38] S. Zhou, L. Zuo, Nonlinear dynamic analysis of asymmetric tristable energy harvesters for enhanced energy harvesting, Commun. Nonlinear Sci. Numer. Simul. 61 (2018) 271–284.